



OPEN ACCESS

EDITED BY

Mary Poupot-Marsan,
INSERM U1037 Centre de Recherche en
Cancérologie de Toulouse, France

REVIEWED BY

Richard Lopez,
Duke University, United States
Emmanuel Scotet,
Institut National de la Santé et de la
Recherche Médicale (INSERM), France

*CORRESPONDENCE

Cindrilla Chumduri
✉ cindrilla.chumduri@bce.au.dk
Dieter Kabelitz
✉ Dietrich.Kabelitz@uksh.de
Thomas F. Meyer
✉ t.meyer@ikmb.uni-kiel.de;
✉ meyer@mpiib-berlin.mpg.de

†These authors have contributed equally to
this work and share first authorship

‡These authors have contributed equally to
this work and share last authorship

RECEIVED 22 August 2023

ACCEPTED 02 November 2023

PUBLISHED 27 November 2023

CITATION

Dong J, Holthaus D, Peters C, Koster S,
Ehsani M, Quevedo-Olmos A, Berger H,
Zarobkiewicz M, Mangler M,
Gurumurthy RK, Hedemann N,
Chumduri C, Kabelitz D and Meyer TF
(2023) $\gamma\delta$ T cell-mediated cytotoxicity
against patient-derived healthy and cancer
cervical organoids.
Front. Immunol. 14:1281646.
doi: 10.3389/fimmu.2023.1281646

COPYRIGHT

© 2023 Dong, Holthaus, Peters, Koster,
Ehsani, Quevedo-Olmos, Berger,
Zarobkiewicz, Mangler, Gurumurthy,
Hedemann, Chumduri, Kabelitz and Meyer.
This is an open-access article distributed
under the terms of the [Creative Commons
Attribution License \(CC BY\)](https://creativecommons.org/licenses/by/4.0/). The use,
distribution or reproduction in other
forums is permitted, provided the original
author(s) and the copyright owner(s) are
credited and that the original publication in
this journal is cited, in accordance with
accepted academic practice. No use,
distribution or reproduction is permitted
which does not comply with these terms.

$\gamma\delta$ T cell-mediated cytotoxicity against patient-derived healthy and cancer cervical organoids

Junxue Dong^{1,2†}, David Holthaus^{1†}, Christian Peters³,
Stefanie Koster², Marzieh Ehsani¹, Alvaro Quevedo-Olmos¹,
Hilmar Berger^{1,2}, Michal Zarobkiewicz^{3,4}, Mandy Mangler^{5,6},
Rajendra Kumar Gurumurthy², Nina Hedemann⁷,
Cindrilla Chumduri^{2,8,9*‡}, Dieter Kabelitz^{3*‡}
and Thomas F. Meyer^{1,2**‡}

¹Laboratory of Infection Oncology, Institute of Clinical Molecular Biology, Christian-Albrechts-Universität zu Kiel and University Hospital Schleswig-Holstein, Kiel, Germany, ²Department of Molecular Biology, Max Planck Institute for Infection Biology, Berlin, Germany, ³Institute of Immunology, Christian-Albrechts-Universität zu Kiel and University Hospital Schleswig-Holstein, Kiel, Germany, ⁴Department of Clinical Immunology, Medical University of Lublin, Lublin, Poland, ⁵Department of Gynaecology and Obstetrics, Vivantes Auguste Viktoria-Klinikum, Berlin, Germany, ⁶Department of Gynaecology, Charité University Medicine, Berlin, Germany, ⁷Department of Gynaecology and Obstetrics, University Hospital Schleswig-Holstein, Kiel, Germany, ⁸Laboratory of Infections, Carcinogenesis and Regeneration, Medical Biotechnology Section, Department of Biological and Chemical Engineering, Aarhus University, Aarhus, Denmark, ⁹Chair of Microbiology, University of Würzburg, Würzburg, Germany

Cervical cancer is a leading cause of death among women globally, primarily driven by high-risk papillomaviruses. However, the effectiveness of chemotherapy is limited, underscoring the potential of personalized immunotherapies. Patient-derived organoids, which possess cellular heterogeneity, proper epithelial architecture and functionality, and long-term propagation capabilities offer a promising platform for developing viable strategies. In addition to $\alpha\beta$ T cells and natural killer (NK) cells, $\gamma\delta$ T cells represent an immune cell population with significant therapeutic potential against both hematologic and solid tumours. To evaluate the efficacy of $\gamma\delta$ T cells in cervical cancer treatment, we generated patient-derived healthy and cancer ectocervical organoids. Furthermore, we examined transformed healthy organoids, expressing HPV16 oncogenes E6 and E7. We analysed the effector function of *in vitro* expanded $\gamma\delta$ T cells upon co-culture with organoids. Our findings demonstrated that healthy cervical organoids were less susceptible to $\gamma\delta$ T cell-mediated cytotoxicity compared to HPV-transformed organoids and cancerous organoids. To identify the underlying pathways involved in this observed cytotoxicity, we performed bulk-RNA sequencing on the organoid lines, revealing differences in DNA-damage and cell cycle checkpoint pathways, as well as transcription of potential $\gamma\delta$ T cell ligands. We validated these results using immunoblotting and flow cytometry. We also demonstrated the involvement of BTN3A1 and BTN2A1, crucial molecules for $\gamma\delta$ T cell activation, as well as differential expression of PDL1/CD274 in cancer, E6/E7+ and healthy organoids. Interestingly, we observed a significant reduction in cytotoxicity upon

blocking MSH2, a protein involved in DNA mismatch-repair. In summary, we established a co-culture system of $\gamma\delta$ T cells with cervical cancer organoids, providing a novel *in vitro* model to optimize innovative patient-specific immunotherapies for cervical cancer.

KEYWORDS

cervical cancer, human papillomavirus, ectocervix, organoids, immunotherapy, $\gamma\delta$ T cells

1 Introduction

According to latest WHO data, cervical cancer is the fourth common cancer among women worldwide (1). The majority of cervical cancers are strongly associated with persistent infection with high-risk oncogenic human papilloma virus (HR-HPV) (2, 3). Among HR-HPVs, HPV16 and HPV18 account for about 70% of cervical cancers (4). Yet, additional infectious agents have also been implicated as co-drivers of cervical cancer (5). Considering that only a quarter of cervical cancer patients respond to chemotherapy, the development of more personalized therapies is urgently needed. Recent advances in organoid technology have enabled the culture of human ectocervical organoids that faithfully replicate healthy and cancerous tissues (6). These organoids serve as a promising *in vitro* model, preserving original cellular heterogeneity and accurately recapitulating epithelial architecture and functionality. Recognizing the absence of *in vitro* models for HPV, we have earlier reported the transformation of healthy cervical organoids with HPV-derived oncogenes E6 and E7 via lentiviral transfer (5). These transformed organoids exhibit significant deviations from their corresponding healthy controls (5).

A numerically minor yet important subset of T lymphocytes in the peripheral blood endowed with anti-cancer activity is $\gamma\delta$ T cells (7, 8). $\gamma\delta$ T cells differ from conventional $\alpha\beta$ T cells in at least two important aspects: (i) $\gamma\delta$ T cells do not recognize peptides presented by MHC class I or class II molecules but rather recognize phosphorylated intermediates (“phosphoantigens”) of the cholesterol synthesis pathway and additional unconventional ligands; and (ii) $\gamma\delta$ T cells do not require MHC molecules for antigen recognition, which opens the possibility of applying $\gamma\delta$ T cells across HLA barriers (9, 10). $\gamma\delta$ T cells express CD3-associated T cell receptors (TCR) composed of γ and δ chains (11, 12). Like other cytotoxic effectors, $\gamma\delta$ T cells directly participate in the elimination of tumour cells, but they also indirectly control the tumour immune response by modulating the activity and functions of other immune cells (7). In healthy adults, approximately 1–5% of circulating T lymphocytes express V δ 2 paired with V γ 9; the proportion of such V δ 2 T cells can rapidly increase during the acute phase of several infectious diseases (11, 12). Recent studies have shed light on the mode of recognition of phosphoantigens (pAg) by $\gamma\delta$ T cells. In this context, an indispensable role of members of the butyrophilin (BTN) family of transmembrane molecules has been discovered. According to the current model, microbe- or tumour-derived pyrophosphates bind to the

intracellular B30.2 domain of BTN3A1 which then interacts with BTN2A1 to induce a conformational alteration of the extracellular BTN3A1/2A1 complex which is recognized by the $\gamma\delta$ TCR (13–16).

$\gamma\delta$ T cells have well-established protective roles in cancer (8, 17, 18). Multiple mouse models have demonstrated their protective role in cancer progression (17, 19). However, previous studies so far have only investigated the effect of $\gamma\delta$ T cells on cervical cancer-derived cancer cell lines and tissue slices (17, 20) or utilized NK cells (21), while studies comparing their effects on patient-derived organoids have not yet been reported. In this study, we provide a model to assess $\gamma\delta$ T cell-mediated cytotoxicity by live cell imaging and flow cytometry-based assays.

2 Methods

2.1 Isolation of cervical tissue and cervical organoid culture

Human cervical specimens were obtained from volunteers undergoing standard surgical procedures at the Department of Gynaecology, Charité University Hospital, and August-Viktoria Klinikum, Berlin (Ethics Approval EA1/059/15 from local authorities), informed consent was obtained from all donors. Samples were processed within 2–3 hours after removal.

Organoids were derived from tissue resection as previously described (5, 6, 22). In short, biopsies were washed and cells were isolated by mincing and enzymatic digestion with 0.5 mg/mL collagenase type II for 2.5 h at 37°C. Afterwards, cells were pelleted at 100g for 5 min (4°C) and then again digested with TrypLE Express Enzyme (Gibco, 12604013) for 15 min at 37°C. Cells were then expanded in collagen-coated T25 tissue culture flasks in cervical organoid medium (Advanced DMEM/F-12 (Gibco, 12634) supplemented with 10 mM HEPES (Capricorn, HEP-B), 1% GlutaMax (Gibco, 35050061), 1x NCS21 Neuronal Supplement (Capricorn, C21-H), 1x N2 (Capricorn, N2-K), 10 ng/mL human EGF (Peprotech, AF-100-15), 0.5 μ g/mL hydrocortisone (Sigma, H0888), 100 ng/mL human noggin (Peprotech, 120-10C), 100 ng/mL human FGF-10 (Peprotech, 100-26-25), 1.25 mM N-acetyl-L-cysteine (Sigma, A9165), 2 μ M TGF- β receptor kinase Inhibitor IV (A83-01, Cayman Chemicals, Cay9001799), 10 μ M ROCK inhibitor (Y-27632, Cayman Chemicals, Cay10005583), 10 mM nicotinamide (Sigma, N0636), 10 μ M forskolin (Sigma, F6886)) until reaching 70–80% confluency.

After successful establishment, cells were harvested and ~20,000 cells were seeded into 50 μ l Matrigel domes (Corning, 11543550).

Organoids were maintained by passaging every 1-2 weeks at a 1:2-1:5 ratio using enzymatic digestion with TrypLE followed by mechanical singularization of cells using a syringe with an 18G needle (BD medical, BDAM303129) as described earlier (22).

2.2 Cell lines and 3T3-J2 irradiation

AGS0 cells (AGS cell line devoid of *parainfluenza virus 5* infection, kindly provided by Richard E. Randall, School of Biology, St. Andrews University) were maintained in RPMI 1640 medium (Capricorn, RPMI-HA) supplemented with 1 mM Sodium pyruvate (Capricorn, NPY-B), 1x Penicillin/Streptomycin and 10% fetal calf serum (Sigma, F7524). HeLa (ATCC CCL-2; RRID : CVCL_0030) and 3T3-J2 cells (kindly provided by Craig Meyers; Howard Green laboratory, Harvard University; RRID : CVCL_W667) were maintained in DMEM (Capricorn, DMEM-HPSTA) supplemented with 1x Penicillin/Streptomycin (Gibco, 15070063), 10 mM HEPES and 10% fetal calf serum (Sigma, F7524). The 3T3-J2 cells were irradiated with 30 Gy in a Gammacell 40 Exactor. After irradiation, 1×10^6 irradiated 3T3-J2 were seeded per T25 Flask and incubated overnight until all cells attached to the surface.

2.3 2D cervical stem cell lines culture

Passage 0 epithelial cells were cultured in plastic cell culture vessels without an irradiated 3T3-J2 monolayer and seeded in a Collagen I (1:100, Fisher Scientific, A1064401) pre-coated T25 flask. After most epithelial cells attached to the surface, the medium was changed every 2-3 days until confluence reached 80-90%. The cells were then passaged at a ratio of 1:2. For the passage 0, the medium was removed and the cells were washed three times with PBS (Capricorn, PBS-1A) and dissociated with 1 mL TrypLE (for each T25 flask) incubating 10 min at 37°C. The cells were detached from the flask surface and the cell suspension was collected with 10 mL Advanced DMEM/F12. After centrifugation at 400g for 4 min at 4°C, the cell pellet was resuspended with cervical organoid medium and seeded on irradiated 3T3-J2 monolayers.

From passage 1, ectocervical epithelial cells were cultured with an irradiated 3T3-J2 layer and the medium was refreshed every 2-3 days. When it reached 80%-90% confluency, the cells were enzymatically detached twice. The first time, 0.5 mL TrypLE was used for each T25 flask for 1 min to detach the 3T3-J2 feeder cells, and then the cervical epithelial cells were detached with another 1 mL TrypLE and incubated for 10 min.

2.4 Whole mount immunofluorescence assays (IFAs) and microscopic analyses

Phase contrast and brightfield images were taken using an IX50 (Olympus) microscope with a 4x or 10x objective. Images were

contrast adjusted and scale bars were added using FIJI (ImageJ; RRID : SCR_002285) (23).

For fluorescent microscopy, organoids were processed as described before (24). In short, organoids were harvested and washed once in PBS, then incubated in cell-recovery solution (Corning, 47743-696) for 30 min, followed by an additional wash with PBS (Capricorn, PBS-1A), and fixed for 20 min in 4% paraformaldehyde (PFA; Carl Roth, P087). Cells were permeabilized with 0.1 M glycine (Carl Roth, 3908), 0.2% Triton-X100 (Carl Roth, 3051) in TRIS-buffered saline (TBS; 50 mM Tris-Cl (Carl Roth, 9090), pH 7.5, 150 mM NaCl (Carl Roth, 3957)) and incubated in blocking buffer consisting of 3% bovine serum albumin (Carl Roth, 3854), 1% normal goat serum (Capricorn, GOA-1A), 0.2% Triton-X-100, and 0.1% Tween-20 (Sigma, P9416) in TBS for 2 h at RT. Primary antibodies were added for incubation at 4°C overnight in blocking buffer and organoids were washed the next day four times with 0.2% Triton-X100, 0.1% Tween-20 in TBS. Secondary antibodies and 10 μ g/mL Hoechst 33342 (Thermo Fisher, H1399) as nuclear stain were added, kept for 1 h at RT in the dark, followed by three additional washing steps with TBS. After a final wash with deionized water, organoids were mounted with Fluoromount-G (Southern Biotech, 0100-01) on glass slides. Images were taken using a cLSM 880 microscope (Zeiss), equipped with Plan-Apochromat 20x/0.8 M27 and C-Apochromat 40x/1.20 water M27 objectives and analysed with ZEN blue software (v3.5; RRID : SCR_013672) and FIJI. Antibodies and dilutions are listed in [Supplementary Table 1](#).

2.5 Isolation of gDNA and real-time quantitative-polymerase chain reaction

For nucleic acid extraction, organoids were harvested, pelleted, and washed with ice-cold PBS. Matrigel was removed by incubation with cell-recovery solution for 30 min at 4°C. Genomic DNA (gDNA) was isolated with the Quick-DNA Miniprep (Zymo, D3024) according to manufacturer's instructions. Purity of DNA was assessed by A260/A280 absorbance ratio using an Infinite M200 Pro plate reader (Tecan). RT-qPCR was performed with a StepOnePlus (Agilent) using the Luna Universal qPCR Master Mix (NEB, M3003), and included initial enzyme activation for 3 minutes at 95°C, followed by 40 cycles of 20s at 95°C, 30s at 60°C and 20s at 72°C. A minimum of 30 ng gDNA was used per well. Melting curve analysis was performed to verify amplicon specificity. Relative expression was calculated using the Δ CT method, and HPV status was assessed by electrophoresis of the amplified products. For that, amplicons were separated on a 1.5% agarose gel containing SYBR Safe Nucleic Acid Gel Stain (Invitrogen, S33102) in 0.5x TRIS-Borate-EDTA (TBE) -buffer (40 mM Tris-Cl, 45 mM boric acid (Carl Roth, P010), 1 mM EDTA (Carl Roth, X986)). The following primers were used:

HPV16-for 5'-AGCTGTCATTTAATTGCTCATAACAGTA-3' (25);

HPV16-rev 5'- TGTGTCCTGAAGAAAAGCAAAGAC-3' (25);

HPV18-for 5'-CGAACCACAACGTCACACAAT-3' (25);

HPV18-rev 5'-GCTTACTGCTGGGATGCACA-3' (25);
 GAPDH-for 5'-GGTATCGTGAAGGACTCATGAC-3' (5);
 GAPDH-rev 5'-ATGCCAGTGAGCTTCCCGTTCAG-3' (5).

Signal was recorded using a ChemiDoc MP Imaging System (Biorad).

2.6 V γ 9V δ 2 T cell expansion

V γ 9V δ 2 T cells were expanded from peripheral blood mononuclear cells (PBMCs) isolated from leukocyte concentrates of healthy blood donors using a Ficoll-Hypaque (Biochrom, Biocoll L 6113/5) density gradient according to the manufacturer's protocol. Leukocyte concentrates were provided by the Institute of Transfusion Medicine UKSH Campus Kiel and were used in an anonymized fashion and Ethics Approval D 434/22 was provided by local authorities. The cell pellet was resuspended in RPMI medium (Capricorn, RPMI-STA) containing 10% FCS (Sigma, F7524). Before expansion, the initial V γ 9V δ 2 T population among CD3+ T cells was checked by staining PBMCs with anti-V δ 2-FITC and anti-CD3-APC. Samples with a V γ 9V δ 2 T cell proportion over 2% were deemed acceptable and the sample was further processed. V γ 9V δ 2 T cells were selectively activated by stimulating PBMCs with 5 μ M zoledronic acid (Novartis) and 50 IU/mL IL-2 (Novartis) over the expansion period of 14 days essentially as described (26). IL-2 was supplemented every other day. Purity of V γ 9V δ 2 T cell lines was checked with anti-V γ 9-FITC and anti-CD3-APC. Lines were used for experiments when V γ 9V δ 2 T cells represented more than 90% of the total cell population. Antibodies and dilutions are listed in [Supplementary Table 1](#).

2.7 V γ 9V δ 2 T cell co-culture with cervical cells

The B-cell lymphoma Daudi cell line (ATCC, CCL-213; RRID : CVCL_0008) with known sensitivity to V γ 9V δ 2 T cell killing (27) was included as positive control. All lines were washed with PBS and pelleted in 15 mL falcon tubes by centrifuging at 1400 rpm for 5 min. Cells were stained with PKH67 (Sigma, PKH67GL) green dye was prepared according to manufacturer protocol. After incubation at RT for 4 min in the dark, 7 mL RPMI medium containing 10% FCS was added and incubated for further 1 min to stop the staining. Cells were used at a ratio of 10:1 (T cells: epithelial cells). Co-culture was performed for 4 hours with the respective surface blocking mAb, if appropriate, and thereafter cells were washed in PBS, and taken up in sample buffer containing 0.2 μ g/mL propidium iodide (PI) for 20 min at 4°C and analysed by flow cytometry. Data was then analysed with FlowJo v10 (RRID : SCR_008520). The absolute number of viable epithelial cells (FITC+PI-) was calculated with the formula derived from Sacchi et al. (28):

$$\text{Cytotoxicity} = 100 - \left[\frac{\% \text{ of living epithelial cells in co-culture with } \gamma\delta \text{ T cells}}{\% \text{ of living epithelial cells without } \gamma\delta \text{ T}} \times 100 \right]$$

2.8 CD107a degranulation assay

50 \times 10³ effector cells were cultured alone or together with 5 \times 10³ tumour cells for 4 h at a 10:1 ratio in the presence of anti-CD107a-PE mAb (clone: H4A3; BD Biosciences) and monensin (3 μ M; added after 1 h). Thereafter cells were washed twice in PBS and analyzed by flow cytometry. Where appropriate, the synthetic pAg bromohydrin pyrophosphate (BrHPP; Innate Pharma) was added at 300 nM to activate V γ 9V δ 2 T cells. Cells were immediately acquired on a BD FACSCanto I flow cytometer. Data was then analysed with FlowJo v10.

2.9 Live cell imaging

Prior to co-culture, a flat-bottom 384 well-plate (black with clear bottom, Corning) was coated with Poly-2-hydroxyethyl methacrylate (poly-HEMA; Sigma, P3932) in 100% ethanol as described earlier (29). 30 μ l poly-HEMA was added in each well and the plate was left to dry overnight under the culture hood. The plate was washed with PBS immediately before use.

The imaging protocol was adapted from previous studies (30, 31). Organoid lines were cultured for around seven days and V γ 9V δ 2 T cells were expanded for 14 days as described above. Matrigel was removed by incubation with cell-recovery solution for 30 min at 4°C. A part of the suspension of organoids was taken and digested into single cells using TrypLE then the number of single cells was counted to estimate organoid equivalents. The organoids were washed with cold PBS and thereafter organoids were collected and stained with CellTrace CFSE Cell Proliferation Kit (Thermo, C34554) according to the supplier's protocol. Then, V γ 9V δ 2 T cells were added again at a ratio 10:1 (T cells: epithelial cells). NucRed Dead 647 ReadyProbe Reagent (Thermo, R37113) was added to distinguish dead and live cells. In the respective conditions, $\gamma\delta$ T cells were activated with 300 nM BrHPP, "Dead cells" were boiled for 10 min at 95°C before the start of the experiment, and 1 mg/mL Puromycin (InVivoGen, ant-pr-1) treated cells served as death control over time. Measurements were performed using the CELLVISTA 4 automated cell imager in combination with the SYBOT X-1000 with CYTOMAT 2 C-LiN system (all SYNENTEC GmbH). Wells were imaged every hour for a total of 8 hours and afterwards fluorescence data and images were extracted with YT-Software (SYNENTEC GmbH) using the Real Cytoplasm (2F) application. The settings were modified to detect all organoids in the green channel and subsequently, the average intensity of the yellow and red signal within each spheroid area was analysed. The following settings were used for different channels. Exciter: Blue (475/28) - Emissionfilter: Green Filter 530nm (530/43), Exciter: Green (529/24) - Emissionfilter: Amber Filter 580nm (607/70), Exciter: Red (632/22) - Emissionfilter: Far Red Filter 670nm (685/40). Scatter plots were assembled in R (v4.1.0) with ggplot2 (v3.4.0).

2.10 Live/dead cytotoxicity assay

1x10⁴ cervical organoid cells were seeded into Collagen I pre-coated 96-well plates without feeder cells. On the next day, cells

were co-incubated with 1×10^5 $\gamma\delta$ T cells (EC : TC = 1:10) for four hours in Opti-MEM (Gibco, 11058021). To quantify dead/live cells, the MultiTox-Glo Multiplex Cytotoxicity Assay kit (Promega, G9272) was used according to manufacturer's instructions. The values were normalized to the respective untreated control, and the ratio of dead/live cells was then normalized to the healthy organoids to obtain fold changes.

2.11 SDS-PAGE and immunoblotting

For SDS-PAGE analysis, organoids were harvested, pelleted, and washed with ice-cold PBS. Matrigel was removed by incubation with cell-recovery solution (Corning) for 1 h at 4°C. Cells were then lysed in RIPA-buffer (50 mM Tris-HCl pH 8.0, 1% w/v NP-40 (Sigma, 492018), 0.5% w/v sodium deoxycholate (Sigma, D6750), 0.1% w/v SDS (Carl Roth, 0183), 150 mM NaCl, and 5 mM EDTA). After assessing the protein content using the Pierce Rapid Gold BCA Protein Assay Kit (Thermo, A53225) samples were diluted with 6x Laemmli buffer (70% v/v Tris HCl pH 6.8, 10% w/v SDS, 30% (v/v) glycerol (Carl Roth, 3783) and 0.01% w/v Bromophenol blue (Sigma, B0126) containing 10% v/v β -mercaptoethanol (Carl Roth, 4227). Samples were boiled at 95°C for 5 minutes. 25 μ g of protein per condition was blotted onto Amersham Protran nitrocellulose membranes (Fisher Scientific, 10600016) using standard techniques and transfer quality was validated by Poinceau S (Sigma, P3504) total protein staining. The membranes were blocked for 1 hour in 1x RotiBlock (Roth, A151) and incubated with primary antibodies overnight. After three washing steps, membranes were incubated with respective peroxidase-conjugated secondary antibodies and signals were detected using chemiluminescence with a ChemiDoc MP Imaging System (Biorad). Antibodies and dilutions are listed in [Supplementary Table 1](#).

2.12 Analysis of bulk RNA sequencing

Quality of raw reads was assessed by FastQC. Reads were mapped to the human reference genome (assembly GRCh37) using the splice aware aligner STAR (v2.7) (32) in two-pass mode. Quality GTF files downloaded from Gencode (v28) (33), were used to map reads into genes with FeatureCounts in order to obtain raw counts. From this matrix of raw counts, genes with no expression across samples were filtered out, and differential gene expression was performed using DESeq2 (v1.32.0) (34) in R (35). Volcano plots were generated using ggplot2 (v3.4.0). Genes were ranked based on their log₂ fold change compared to healthy controls, and gene set enrichment analysis (GSEA) was performed using the fgsea implementation from the clusterProfiler R package (v4.0.5) (36). Gene sets from Hallmark (H), Curated Gene Sets (C2) and GO Biological Process (C5-BP), retrieved from MsigDB (37) using msigdb (v7.5.1) were studied. The gene expression heatmaps of the TPMs were generated using the pheatmap package (v1.0.12). Principal Component Analysis (PCA) was performed on the TPM normalized counts and the plots were generated using factoextra (v1.0.7) on the result of the pca

function in base R. All the analyses were performed in R (v4.1.0). RNA-seq DGE and GSEA analysis results are included in [Table 1](#).

2.13 Statistical analysis and panel composition

Basic calculations were performed using MS EXCEL 2016 (Microsoft). Figures were plotted using Prism 10 (GraphPad) or R (v4.1.0). P values \leq 0.05 were considered statistically significant. Asterisks indicate statistical significance values as follows: * p < 0.05, ** p < 0.01, *** p < 0.001, **** p < 0.0001. The panel composition and annotations were created using Affinity Designer 2.1.1 (Serif).

3 Results

3.1 Ectocervical organoids accurately represent the phenotype of the parental tissue

To establish a suitable model mimicking ectocervical tissue, we have established patient-derived organoids (PDOs) cervical tissues in our earlier studies (5, 6, 22). These lines were grown in T25 tissue flasks on irradiated 3T3-J2 mouse fibroblast feeder cells and subsequently embedded in Matrigel to generate 3D organoids ([Figure 1A](#)). In order to create paired HPV E6E7-positive lines (referred to as HPV+), the healthy organoid lines were transformed with a construct containing human papilloma virus (HPV) oncogenes E6 and E7 as described earlier (5, 22). We were able to passage all lines for approximately 20 passages prior to growth arrest. Visual inspection under brightfield microscopy revealed no discernible phenotypic difference between healthy, HPV+ and cancer lines ([Figure 1B](#)). Amplification of integrated HPV16 E6E7 oncogenes was detected by PCR of genomic DNA in the HPV+ and cancer organoids ([Figure 1C](#)). Since HPV16 and 18 are the most common causes of cervical cancers, we also assessed the HPV18 status in our organoids. HPV18 was detected in one of the lines (Cancer D3), also reflecting the naturally occurring ratio of HPV16 and HPV18 infections of two to one (38). HPV18 primer sensitivity was verified using HeLa cells as a positive control ([Figure 1C](#)). We have summarized the characteristics of the organoid lines in [Table 1](#).

To validate the ectocervical nature of our organoids, we next characterized the organoid lines for marker gene expression and localization by whole mount immunofluorescence assays. All lines were positive for cytokeratin 5 (KRT5), a marker of ectocervix, in the outer layers of the organoids resembling the *in vivo* stratified squamous epithelium of the parental tissue. As the basal layer is responsible for proliferation *in vivo*, marker of proliferation KI67 (KI67)-positive cells are expected in this layer. Interestingly, KI67-positive cells were indeed detected in the parabasal layers of healthy PDOs, while they were located throughout the whole organoid for HPV+ and cancer-derived lines ([Figure 1D](#)). A more detailed characterization of ectocervical organoid cultures has been previously provided in our studies (5, 6). Thus, the organoids

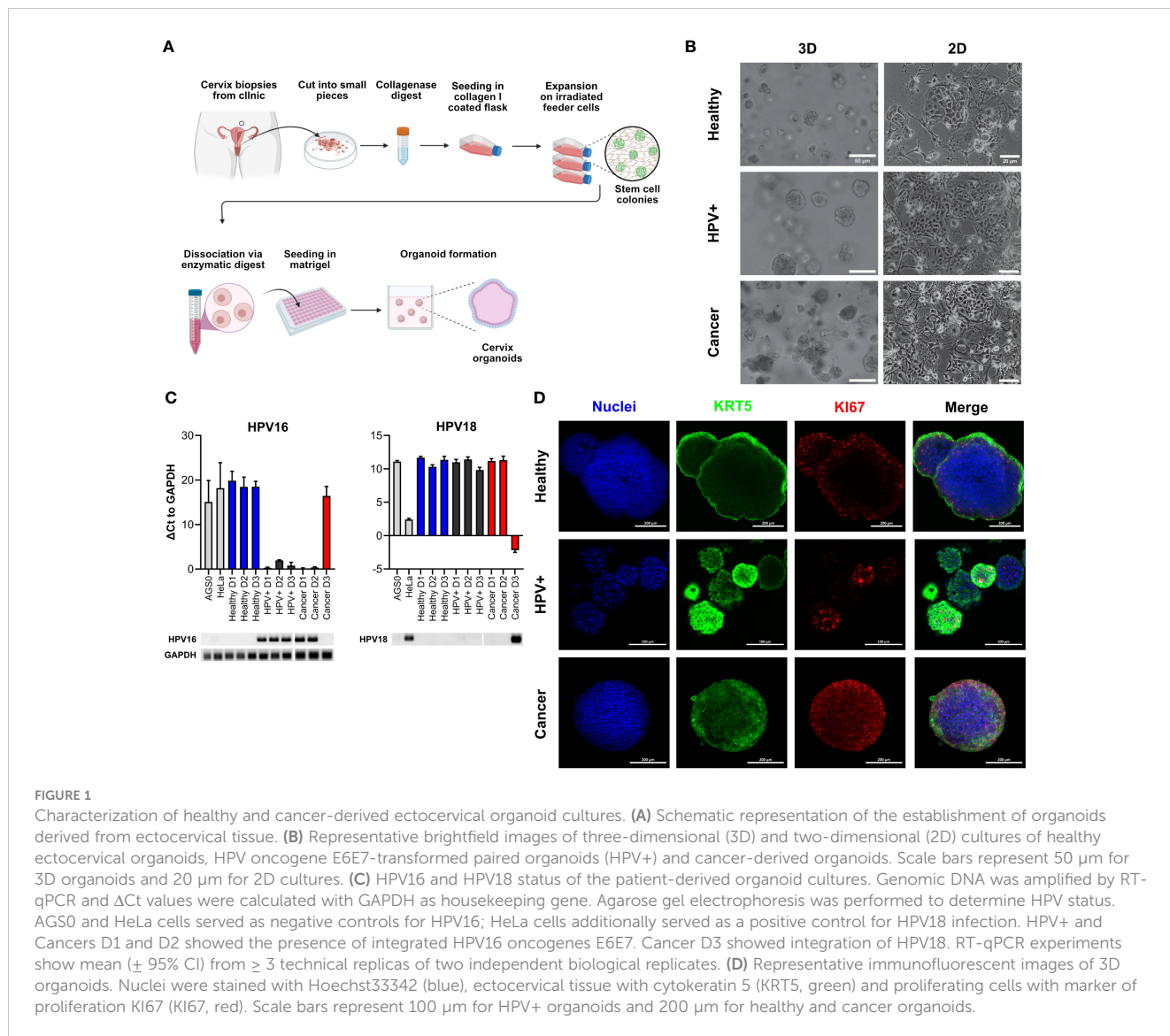


TABLE 1 Characteristics of the organoid lines.

ID	Age at surgery	Disease	HPV16/18 status
Healthy Donor 1	58	not applicable	HPV16/18 free
Healthy Donor 2	51	not applicable	HPV16/18 free
Healthy Donor 3	48	not applicable	HPV16/18 free
Cancer Donor 1	35	Squamous cell carcinoma	HPV16+
Cancer Donor 2	54	Squamous cell carcinoma	HPV16+
Cancer Donor 3	61	Squamous cell carcinoma	HPV18+

HPV+ are derived from the respective healthy lines.

reflect the *in vivo* phenotypes of healthy and cancerous ectocervical tissues.

3.2 $\gamma\delta$ T cells exhibit enhanced killing of HPV+ and cancer-derived organoids

$\gamma\delta$ T cells are an important subset of T lymphocytes involved in anti-tumour immunity. They can kill tumour target cells by the secretory pathway via the release of perforin and granzymes as well as by death receptor pathways (e.g. Fas/Fas-ligand) (11). To first assess whether the tissue identity is also reflected in the immune response of tumour-killing T cell subsets, we co-incubated *in vitro* expanded V γ 9V δ 2 T cells with healthy, HPV+ and cancer-derived organoid lines. Before co-incubation, the purity of $\gamma\delta$ T cell lines was assessed; only cultures with > 90% $\gamma\delta$ T cells were used. Representative examples of purity determinations as analysed by flow cytometry are presented in Supplementary Figure 1. To determine $\gamma\delta$ T cell-mediated cytotoxicity, organoids were stained

with NucRed Dead 647 (Yellow: general stain, Red: dead cells) as previously described for breast cancer-PDOs (31). This staining enabled the detection of an increasing number of dead cells within the organoid population by automatized live cell imaging. Live cell imaging revealed distinct responses of $\gamma\delta$ T cells to HPV+ and cancer-derived organoid lines after four hours of co-incubation (Figures 2A–C). The average accumulation of red stained dead cells in these groups was higher in comparison with healthy organoids, as shown by an increased ratio of Dead/Live signal (Figures 2A–C). When visualizing individual organoid's Dead/Live (Red/yellow) ratios as scatter plots, a clear shift to the Red/Dead signal was observable in cancer and HPV+ organoids when co-incubated $\gamma\delta$ T

cells, even in the absence of the pAg BrHPP (Figure 2B). We observed a significant increase in the ratio of red/dead to yellow/live signal in cancer and HPV+ organoids in comparison to healthy organoids after 4 hours after analysing single organoids (Figure 2C). Consistently, additional activation of $\gamma\delta$ T cells by BrHPP resulted in enhanced cytotoxicity in all organoid lines (Figure 2B; Supplementary Figure 2). Unmerged scatters plots for untreated, unstained, puromycin-treated and dead cells are provided in Supplementary Figure 2. To further confirm the findings, organoid-derived cells were co-incubated with $\gamma\delta$ T cells and cytotoxicity was assessed by an alternative, protease-based cytotoxicity assays after 4h. Higher cytotoxicity was again

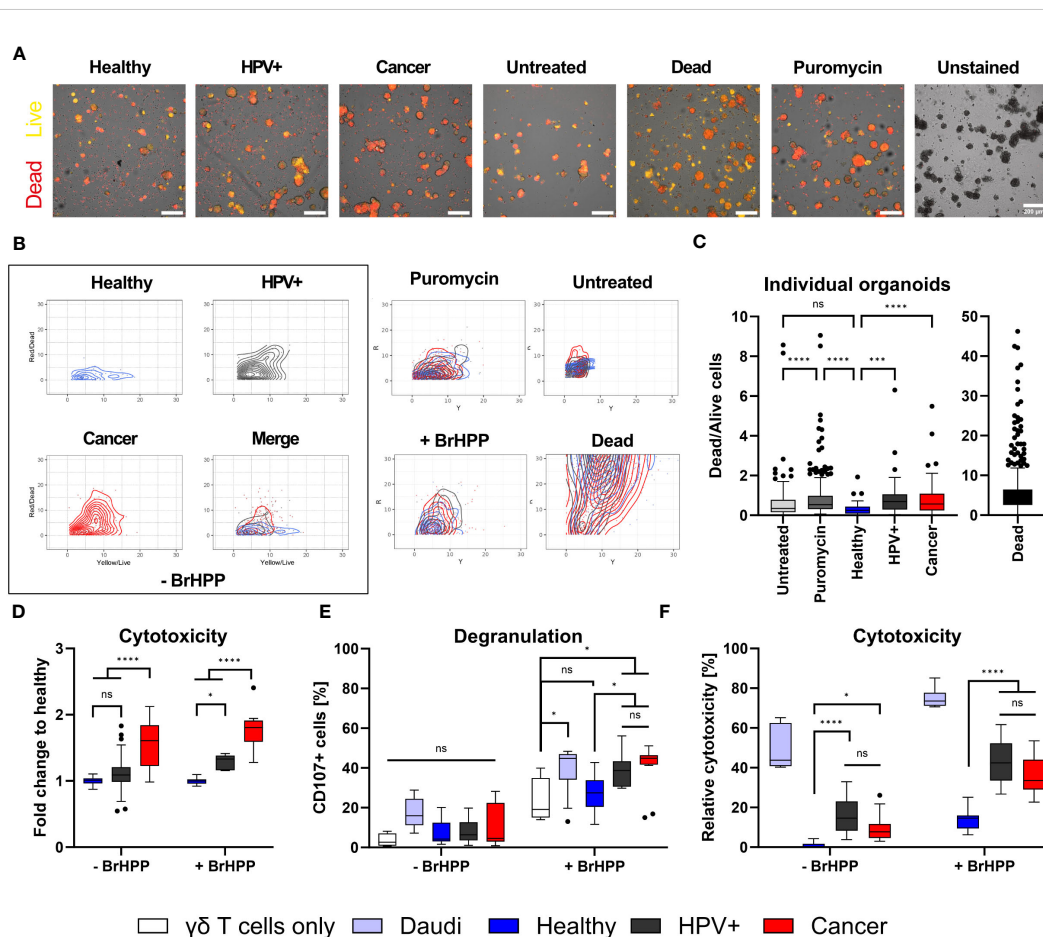


FIGURE 2

$\gamma\delta$ T cells specifically target HPV-positive and cervical cancer organoids. (A) Representative fluorescent images of ectocervical organoids either untreated or co-incubated with $\gamma\delta$ T cells for four hours. $\gamma\delta$ T cells were activated with 300 nM BrHPP, “Dead cells” were boiled for 10 min at 95°C before start of the experiment, and Puromycin-treated cells served as death control over time. Cells were stained with NucRed Dead 647 Ready Probe Reagent. Yellow marks viable cells, red marks dead cells. Scale bars represent 200 μ m. The experiment was performed at least twice with similar results. (B) Scatter plots of dead/live (red/yellow) cell staining in individual organoids show the increasing shift of yellow to red staining of HPV+ and cancer organoids. Merge of all conditions for organoids incubated with $\gamma\delta$ cells in the absence of 300 nM BrHPP is seen in the box at the lower right. Merges of the control conditions are given. Unmerged control conditions are depicted in Supplementary Figure 2. (C) Ratio of dead/live (red/yellow) cell staining of individual organoids after four hours. Organoids with a ratio > 10 were excluded from the graph for visual purposes. Data shows \geq 40 organoids per condition. Statistical significance between conditions was determined using a Kruskal-Wallis test with Dunn’s correction for multiple testing. *** p < 0.001 **** p < 0.0001 (D) Quantification of cytotoxicity measured by MultiTox-Glo Multiplex Cytotoxicity Assay after four hours of co-incubation of organoids with $\gamma\delta$ T cells in the absence or presence of 300 nM BrHPP as indicated. Data was normalized to untreated or BrHPP-treated controls and the ratio of dead/live cells was calculated; fold-change to healthy control was assessed. Data is derived of 12–20 replicates per condition from two independent experiments. (E) Quantification of degranulation of $\gamma\delta$ T cells by CD107a staining with and without additional activation of $\gamma\delta$ T cells by BrHPP using flow cytometry. The B lymphoma cell line Daudi was included as a positive control. Data shows four independent experiments. (F) Quantification of cytotoxicity induced by $\gamma\delta$ T cells by propidium iodide (PI) staining with and without activation of $\gamma\delta$ T cells by BrHPP using flow cytometry. Data shows \geq three independent experiments run in triplicates. All box plots show Median with Tukey whiskers. Statistical significance in (D–F) was determined using a Two-Way ANOVA with Tukey’s correction for multiple testing. ns not significant * p < 0.05 **** p < 0.0001.

observed in cancer PDOs after co-incubation with unstimulated $\gamma\delta$ T cells (Figure 2D, left), while treatment with BrHPP additionally resulted in a significant increase in $\gamma\delta$ T cell-mediated cytotoxicity against HPV-transformed organoids and cancer lines (Figure 2D, right).

To confirm the differences in $\gamma\delta$ T-mediated cytotoxicity induced by $\gamma\delta$ T cells against healthy and HPV+ and cancer-derived cervical organoids, we determined degranulation/Lamp-1 mobilization of $\gamma\delta$ T cells by flow cytometry. As positive control we included the B lymphoblast cancer cell line Daudi. As expected, we could show that the addition of BrHPP significantly enhanced degranulation in all conditions (Figure 2E, right). However, the addition of BrHPP also resulted in a significant increase in degranulation of HPV+ and cancer organoids in comparison with healthy controls (Figure 2E). Confirming our previous results using an alternative cytotoxicity read-out, we demonstrated that unstimulated $\gamma\delta$ T cells already exhibit significantly increased cytotoxic activity against cancer and HPV+ cells in comparison to healthy controls as measured by propidium iodide (PI) staining to detect dead cells (Figure 2F). Again, the addition of BrHPP increased the overall response and significantly enhanced the killing of HPV+ and cancer organoids as compared to healthy cells (Figure 2F).

3.3 Transcriptomic and protein analysis reveals differences in molecules relevant for $\gamma\delta$ T cell activation

We have observed significant differences in $\gamma\delta$ T cell-mediated cytotoxicity against distinct organoid lines. To identify putative underlying factors facilitating increased cytotoxicity on cancer and HPV+ organoids, explorative bulk RNA-sequencing (RNAseq) was conducted. Gene expression analysis revealed differences between conditions and also between patient isolates (Figure 3A; Table 1). Cancer lines exhibited comparable expression of genes that were distinguishable from the other conditions, as shown by the first principal component (Figure 3A; Supplementary Figure 3). Isolates transformed with HPV oncogenes E6E7 grouped as intermediates between healthy and cancer organoids (Figure 3A; Supplementary Figures 3, 4). HPV+ isolates generally moved into the cancer direction on the first principal component. Interestingly, the transformation of HPV+ D3 resulted in a clear shift in the second principal component from the other lines. Differential gene expression analysis showed a strong upregulation of cell proliferation-associated genes in the HPV transformed isolates such as *CDC7*, *MCM6/7*, and *RFC3* (Figure 3B; Supplementary Material Table 1). It is notable that there is a clear bias of upregulation of genes in the HPV+ condition in comparison with healthy organoids (Figure 3B). Cancer organoids showed an upregulation of pathways involved in DNA-damage, cell cycle checkpoint, and DNA-binding/modification pathways and downregulation of pathways involved in differentiation of squamous epithelia (Figure 3B; Supplementary Figure 4; Table 1). No significant elevation of antiviral/IFN-associated pathways was detected.

Having gained insights into the differential expression of transcripts between conditions we further explored the possible underlying mechanisms of enhanced killing of HPV+ and cancer organoids. For this, we investigated the expression of putative $\gamma\delta$ T cell ligands and molecule involved in $\gamma\delta$ T cell activation (Figure 3C) as summarized in Kabelitz et al. (11). As expected, we observed pronounced differences in expression patterns between the conditions. Upon transformation with E6E7 gene expression patterns of healthy organoids shifted more towards the cancer direction. Some molecules associated with $\gamma\delta$ T cell activation such as the *Butyrophilin (BTN)*-family, *UL16 Binding Protein (ULBP)*-family, *MHC Class I Polypeptide-Related Sequence A (MICA)* and *B (MICB)*, *Annexin A2 (ANXA2)*, and *Apolipoprotein A1 (APOA1)* were lower in cancer organoids. In contrast, others such as *protein C receptor (PROCR)*, and *ATP Synthase Peripheral Stalk-Membrane Subunit B (ATP5F1/BP)* were expressed in a higher amount than healthy controls (Figure 3C). CD1d was only highly expressed in Cancer D3.

In addition to the well characterized genes involved in $\gamma\delta$ T cell activation, we also investigated the regulation of other genes such as members of the *human MutS homologue (MSH)*-family, *heat shock protein family D (Hsp60) member 1 (HSPD1)* and *Killer Cell Lectin Like Receptor G2 (KLRG2)*. These genes have been described to play a role in DNA mismatch repair or are involved in stress signalling of cells (39, 40). Interestingly, ectopically expressed *MSH2* has been previously identified as a target for human V γ 9V δ 2 $\gamma\delta$ T cells (11, 39, 41, 42). We found these genes to be upregulated in HPV+ and cancer organoids (Figure 3C). Another highly upregulated gene was found to be *Butyrophilin-Like Protein 9 (BTNL9)* which has been implicated to be of prognostic significance in various cancer types (43, 44). Its potential involvement in the regulation of $\gamma\delta$ T cell mediated killing of tumour cells is unknown but deserves further investigation in light of our current findings with HPV-transformed and cancer organoids. Additionally, *programmed cell death ligand 1 (PD-L1/CD274)* was significantly downregulated in cancer organoids. The PD-L1 receptor PD1 conveys a negative signal on T cells. (45). PD-L1 downregulation might therefore support the enhanced killing of cancer cells by $\gamma\delta$ T cells.

To confirm whether the regulation of transcripts could be translated into protein expression, we analysed the protein expression of selected differentially expressed genes by western blotting (Figure 3D). We confirmed that KI67 was elevated in cancer-derived organoids, consistent with earlier reports (46) and as was observed in immunofluorescence (Figure 1D). Additionally, expression of *MSH2* was upregulated in HPV+ and cancer organoids and PD-L1 was downregulated in cancer organoids in comparison with healthy controls, pointing to possible functional differences in $\gamma\delta$ T cell-mediated killing. As PD-L1 needs to be expressed on the cell surface to fulfil its function, we also conducted flow cytometry to confirm our western blotting and RNA-sequencing results, which, indeed, confirmed decreased surface expression of PD-L1 in cancer organoid isolates (Figure 3E).

Next, we addressed the functional relevance of some of the above molecules for $\gamma\delta$ T cell-mediated killing of HPV+ and cancer organoids. To this end, we co-incubated organoids with expanded $\gamma\delta$ T cells with BrHPP in the absence or presence of blocking

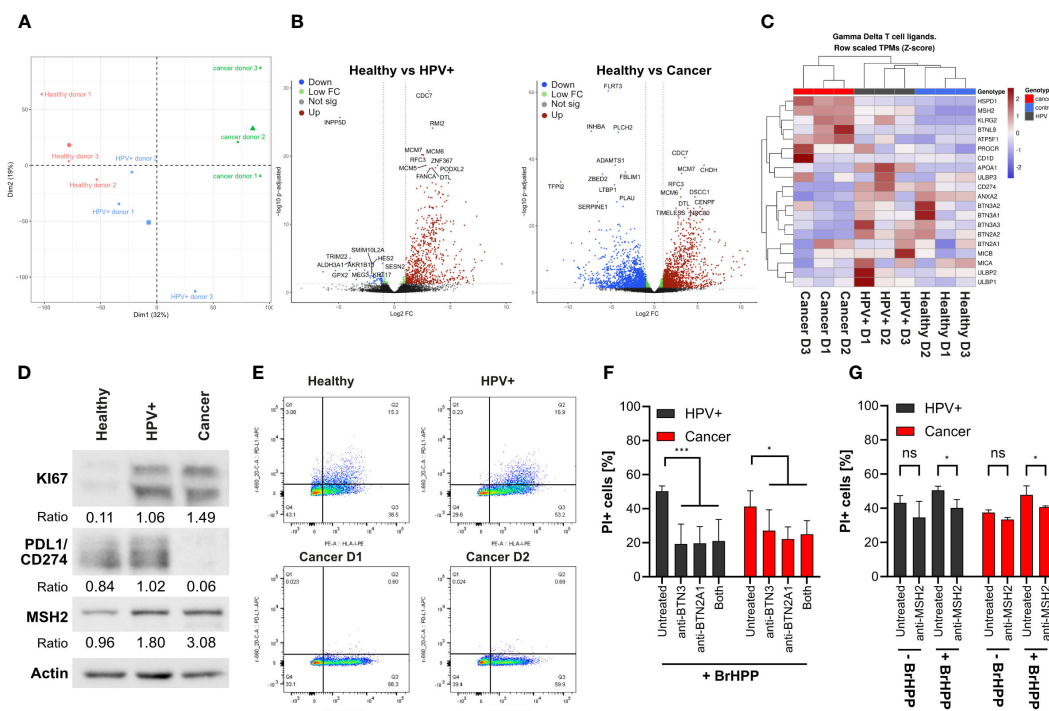


FIGURE 3
 $\gamma\delta$ T cell mediated killing is partially mediated by BTN family members and MSH2. **(A)** PCA analysis of bulk RNA sequencing of the organoid lines. **(B)** Volcano plots of differential gene expression analysis, showing mean Log2 fold-change vs $-\log_{10}$ adjusted p values. HPV16 integration alters the organoid transcriptome. RNA sequencing was performed for 3 independent patient organoid isolates per condition. Downregulated genes are marked in blue, differentially regulated genes with higher p values in green, not significantly regulated genes in grey, and upregulated genes in red. Top10 most significantly up- and downregulated genes are highlighted. **(C)** Heatmap of the gene expression of $\gamma\delta$ T cell ligands highlighting the downregulation of BTN family members and the upregulation of DNA damage associated molecules in the cancer isolates. **(D)** Confirmation of RNaseq results by Western blotting highlighting the differential expression of selected proteins in cancer organoids. **(E)** Dot plot of PDL1/CD274 (Y axis) and HLA class I (X axis) expression analysed by flow cytometry on organoids as indicated, confirming protein expression results in **(D)**. **(F)** Quantification of cytotoxicity in organoid lines by propidium iodide staining with and without blocking antibodies for BTN2A1/3 by BrHPP activated $\gamma\delta$ T cells using flow cytometry. Data shows mean (\pm 95% CI) of three independent experiments. **(G)** Representative quantification of a flow cytometry experiment using anti-MSH2 antibody (2-4 replicates per condition). The percentage of propidium iodide-positive cells is shown. Statistical significance in F and G was determined using a Two-Way ANOVA with Tukey's correction for multiple testing. ns not significant * $p < 0.05$ *** $p < 0.001$.

antibodies against BTN2A1 and BTN3A1 (Figure 3F). While the inhibitory anti-BTN3 antibody used here (clone 103.2) does not discriminate between isoforms BTN3A1/A2/A3 (47), the isoform critically involved in $\gamma\delta$ T cell activation is BTN3A1 (48). We found that blockade of BTN2A1 or/and BTN3A1 significantly reduced killing in all conditions as was in line with earlier reports (49). However, blocking in cancer organoids seemed to be slightly less affected than in HPV+ organoids (Figure 3F). In view of the results shown in Figures 3C, D, we also addressed the potential role of MSH2 which has been identified by Dai et al. (39) as a $\gamma\delta$ T-cell ligand when ectopically expressed on the surface of tumour cells. Blocking of MSH2 by antibodies led to an overall decrease of $\gamma\delta$ T cell-mediated cytotoxicity, most notably against cancer organoids in the presence of BrHPP (Figure 3G). Blocking could decrease $\gamma\delta$ T cell-mediated cytotoxicity of BrHPP activated $\gamma\delta$ T cells to the level of unstimulated $\gamma\delta$ T cells (Figure 3G). While the inhibitory effect of anti-MSH2 antibody blocking was much lower than the effect of anti-BTN2A1/3A1 antibodies, our results suggest that multiple ligand-receptor interactions are involved in the organoid- $\gamma\delta$ T-cell interaction.

In summary, we have identified multiple possible target molecules and pathways that may contribute to enhanced the killing of HPV-infected cervical tissue by $\gamma\delta$ T cells. While the precise role of some molecules (including BTNL9) requires further investigation, the currently established organoid- $\gamma\delta$ T cell co-culture system should prove useful for testing additional modulators (e.g. small molecules, antibodies, tumour sensitizers, etc.) with the ultimate goal of improving the efficacy of $\gamma\delta$ T cell immunotherapy for cervical cancer.

4 Discussion

The association between HPV infection and the onset and the development of cancer has been extensively studied since almost 50 years (50). However, there has been a lack of suitable models that accurately represent and maintain the characteristics of cervical tissue. Previous studies have relied on immortalized cell lines or tissue slices (20). Here, we present a model to study the interaction of tumour-reactive T lymphocyte populations with healthy,

matched HPV16 E6E7 transformed, and cancer-derived primary ectocervical tissues. To achieve this, we utilized an earlier established human ectocervical organoid model including paired HPV16 E6E7 transformed organoids (5, 6). We detected infection-specific differences in proliferation patterns of healthy and HPV-infected organoids by staining with KI67 antibody. Healthy controls exhibited proliferating cells only in the parabasal regions of organoids, cancer organoids showed a wider distribution of proliferation while HPV+ showed an intermediate phenotype. Similar was observed in HPV+ tissue and cancer biopsies confirming the preservation of tissue origin characteristics (46, 51).

$\gamma\delta$ T cells play a distinct role in the immune surveillance against virally infected (including HPV) cells and tumour cells (3, 8, 11, 52). They are believed to be important in the cervical defence against HPV infection (3, 53). To establish an *in vitro* model for in-depth analysis, we co-incubated organoid-derived cells with *in vitro* expanded V γ 9V δ 2 $\gamma\delta$ T cells isolated from healthy donors. In view of the HLA independence of $\gamma\delta$ T cells, the use of allogeneic $\gamma\delta$ T cells from healthy donors is a valuable approach also from a translational perspective. In fact, the adoptive transfer of allogeneic $\gamma\delta$ T cells from healthy donors has already been applied in phase I studies with no major adverse reactions (10). It was thus possible to compare responses of $\gamma\delta$ T cells to healthy, HPV-transformed as well as tumour organoids. Our results demonstrated elevated responses of unstimulated and phosphoantigen-activated $\gamma\delta$ T cells to HPV-infected cells in comparison to healthy controls, independently of the type of assay used. Live cell imaging, protease-dependent cytotoxicity assays, and flow cytometry-based cytotoxicity and degranulation assays demonstrated elevated responses to HPV+ and/or cancer organoids. However, the observed differences in the potency of the assays might reflect differential involvement of the secretory (perforin and granzyme-dependent) and death receptor pathways (e.g., TRAIL, Fas/CD95). It is well known that $\gamma\delta$ T cells can utilize both pathways to kill tumour targets (54, 55). The organoid co-culture system established in our current study will allow us to dissect the precise mechanisms of killing of cancer versus HPV-infected organoids by $\gamma\delta$ T cells in future studies. This will also include the analysis of soluble mediators such as TRAIL, Fas-ligand, granzyme B, IFN γ , and others.

To unravel possible mechanisms behind the responses of $\gamma\delta$ T cells to HPV16-infected organoids, we conducted bulk RNA sequencing. The RNAseq revealed differences between HPV infected vs healthy controls. Importantly, HPV-transformed organoids displayed an intermediate state between healthy and cancer organoids with replicating some, but not all patterns of cancer tissue. Consistent with earlier studies we detected evidence for HPV16-induced DNA damage (5, 56). Interestingly, HPV-induced antiviral responses including the type I interferon pathway were negligible in the pathway analysis. Dekkers et al. (31) have earlier reported a high association between cancer cell killing and the preservation of tumour-specific inflammatory features in breast cancer organoids. In their study, sensitivity to cancer metabolome-sensing engineered T cells (TEGs) was highly associated with the expression of antiviral genes such as *MX1*, *IFIT1*, *OASL* and *XAF1* (31).

Our pathway analysis demonstrated some overlap in DNA-modification pathways and $\gamma\delta$ T cell ligands or associated molecules

between cancer and HPV+ conditions. We reproduced earlier reports (57, 58) of altered transcription and expression of genes such as *TTK protein kinase (TTK)*, *maternal embryonic leucine zipper kinase (MELK)*, *forkhead box M1 (FOXM1)*, *mismatch repair enzyme as mutS homolog 2 (MSH2)*, *matrix metalloproteases (MMPs)* and *programmed cell death ligand 1 (PD-L1/CD274)*. While up-regulation of *PD-L1* is typically associated with poorer outcomes in chemotherapy treatment (58), it was almost absent in our cancer isolates. While exhaustion the role of *Programmed Cell Death 1 (PD-1/CD279)*, *Hepatitis A Virus Cellular Receptor 2 (TIM3/HAVCR2)*, *Lymphocyte Activating 3 (LAG3)* and other checkpoint molecules has been less studied in $\gamma\delta$ T cells compared to conventional $\alpha\beta$ T cells (59), the low to absent PD-L1 expression on cancer organoids may favour persistent effector activity of $\gamma\delta$ T cells. Interestingly, the expression of BTN-family members including *BTN2A1/3A1*, crucial in pAg-mediated $\gamma\delta$ T cell activation was largely down-regulated in the cancer isolates. However, our blocking studies using inhibitory antibodies against *BTN2A1* and *BTN3A1* clearly indicated the significance of these BTN molecules in triggering the cytotoxic activity of $\gamma\delta$ T cells against HPV+ and cancer organoids, in line with previous reports (49). While not directly measured in our study, it can be assumed that HPV+ and cancer organoids produce increased amounts of endogenous pAg isopentenyl pyrophosphate (IPP), leading to *BTN2A1/3A1*-dependent $\gamma\delta$ T cell activation and subsequent tumour cell killing (8, 11, 60). It is noteworthy, however, that blocking of *BTN2A1/3A1* pathways by inhibitory antibodies only partially reduced the killing of organoids. Given that such antibody blockade completely wipes out all phosphoantigen-mediated activation of human $\gamma\delta$ T cells, this strongly suggests that other pathways are involved in organoid- $\gamma\delta$ T cell interaction, one of which might be *MSH2*. Additionally, transcripts of *BTNL9* and cellular stress molecules *HSPD1*, *KLRG2*, and DNA damage associated molecule *MSH2* were upregulated in cancer organoids. While the roles of *HSPD1* and *KLRG2* play a role in regulating $\gamma\delta$ T cell-mediated cytotoxicity in cancer have been described (61, 62), there is limited information about the involvement of *BTNL9* in $\gamma\delta$ T cell-mediated killing of cancer cells. Given our results, further investigation is warranted. Moreover, the upregulation of *MSH2* may be functionally relevant. *MSH2* ectopically expressed on the surface of tumour cells has been identified as a ligand for the human V γ 9V δ 2 TCR (39, 41, 42). Our study demonstrated that the killing of HPV+ and cancer organoid cells by BrHPP-activated $\gamma\delta$ T cells was reduced in the presence of anti-*MSH2* antibody, supporting the hypothesis that the increased levels of *MSH2* contribute to sensitizing of HPV+ and cancer organoid cells to cytotoxicity mediated by $\gamma\delta$ T cells. Taken together, our findings suggest that *BTN2A1/3A1* and *MSH2* are involved in triggering the cytotoxic activity in $\gamma\delta$ T cells towards HPV+ and cancer organoids, but additional pathways might be involved.

In summary, we have established a suitable model to study cellular immune responses to healthy, HPV-transformed and cancerous ectocervical tissue using organoids in combination with short-term expanded $\gamma\delta$ T cells. Co-incubation of organoid-derived cells with $\gamma\delta$ T cells resulted in enhanced killing of HPV-transformed and cancer organoids. We demonstrated the

involvement of BTN-family members BTN2A1/3A1 in $\gamma\delta$ T cell-mediated cytotoxicity and obtained evidence for the additional involvement of human MutS homologue (MSH)-family member MSH2. The presented *in vitro* model will be highly valuable for in-depth analysis of additional pathways and mechanisms of how to enhance $\gamma\delta$ T cell effector function with the ultimate goal of improving $\gamma\delta$ T cell immunotherapy of cervical carcinoma. Such strategies might include (but are not restricted to) sensitizing cancer cells with $\gamma\delta$ T cell activating drugs like zoledronate (63), bispecific $\gamma\delta$ T cell engagers (64), or agonistic anti-BTN3A1 antibodies (65).

Data availability statement

The original contributions presented in the study are publicly available. The data can be found under GSE246571 in GEO at <https://www.ncbi.nlm.nih.gov/geo/query/acc.cgi?acc=GSE246571>.

Ethics statement

The studies involving humans were approved by the ethical committees of the Charité Berlin and the Medical Faculty of the Christian-Albrechts-Universität zu Kiel. The studies were conducted in accordance with the local legislation and institutional requirements. The participants provided their written informed consent to participate in this study.

Author contributions

JD: Formal analysis, Investigation, Methodology, Validation, Visualization, Writing – review & editing. DH: Data curation, Formal analysis, Investigation, Methodology, Supervision, Visualization, Writing – original draft, Writing – review & editing. CP: Formal analysis, Investigation, Methodology, Resources, Supervision, Writing – review & editing. SK: Methodology, Resources, Writing – review & editing, Validation. ME: Data curation, Formal analysis, Investigation, Validation, Writing – review & editing. AQ-O: Data curation, Formal analysis, Investigation, Software, Validation, Visualization, Writing – review & editing. HB: Data curation, Formal analysis, Investigation, Methodology, Software, Writing – review & editing. MZ: Data curation, Formal analysis, Investigation, Methodology, Writing – review & editing. MM: Methodology, Resources, Writing – review & editing. RKG: Conceptualization, Methodology, Resources, Writing – review & editing. NH: Methodology, Project administration, Supervision, Writing – review & editing. CC: Funding acquisition, Methodology, Project administration, Resources, Supervision, Writing – review & editing. DK: Methodology, Project administration, Supervision, Writing – review & editing. TFM: Funding acquisition, Project administration, Resources, Supervision, Writing – review & editing.

Funding

The author(s) declare financial support was received for the research, authorship, and/or publication of this article. TFM acknowledges funding from BMBF Infect-ERA project “CINOCA” (FK 031A409A) and ERC Advanced grant “MADMICS” ID: 885008. JD received a fellowship from CSC and ME is a recipient of the Focus Biomed Foundation. DK was supported by DG grant Ka 502/19-3. The work was supported by the Department of Molecular Biology at MPIIB. CC acknowledges funding from DFG GRK2157 and DFG CH2527/2-1. The authors acknowledge support from the Max Planck Society for covering the Article Publishing Fees via the Central Invoicing agreement with Frontiers.

Acknowledgments

We thank Saskia F. Erttmann for valuable discussions and critical comments on the manuscript. We thank Daniela Wesch, Institute of Immunology, UKSH Kiel for her support in obtaining leukocyte concentrates from blood bank donors. We thank Wiebe Schaefer, Reinhild Geisen, and Anna Willms from SYNENTEC GmbH for the provision of the Cellavista 4 automated cell imager, the SYBOT X-1000, the CYTOMAT 2 C-LiN system, and technical assistance throughout the live cell experiments. We thank ImCheck Therapeutics for kindly providing antagonistic anti-BTN antibodies. Overview schematics were assembled in BioRender.com.

Conflict of interest

The authors declare that the research was conducted in the absence of any commercial or financial relationships that could be construed as a potential conflict of interest.

Publisher's note

All claims expressed in this article are solely those of the authors and do not necessarily represent those of their affiliated organizations, or those of the publisher, the editors and the reviewers. Any product that may be evaluated in this article, or claim that may be made by its manufacturer, is not guaranteed or endorsed by the publisher.

Supplementary material

The Supplementary Material for this article can be found online at <https://www.frontiersin.org/articles/10.3389/fimmu.2023.1281646/full#supplementary-material>

References

- World Health Organisation. *Cervical cancer - Factsheet* (2023). Geneva: WHO. Available at: <https://www.who.int/news-room/fact-sheets/detail/cervical-cancer> (Accessed 20.03.2023).
- Okunade KS. Human papillomavirus and cervical cancer. *J Obstet Gynaecol* (2020) 40:602–8. doi: 10.1080/01443615.2019.1634030
- Dogan S, Terzioglu E, Ucar S. Innate immune response against HPV: Possible crosstalk with endocervical gammadelta T cells. *J Reprod Immunol* (2021) 148:103435. doi: 10.1016/j.jri.2021.103435
- Serrano B, De Sanjose S, Tous S, Quiros B, Munoz N, Bosch X, et al. Human papillomavirus genotype attribution for HPV6, 11, 16, 18, 31, 33, 45, 52 and 58 in female anogenital lesions. *Eur J Cancer* (2015) 51:1732–41. doi: 10.1016/j.ejca.2015.06.001
- Koster S, Gurumurthy RK, Kumar N, Prakash PG, Dhanraj J, Bayer S, et al. Modelling Chlamydia and HPV co-infection in patient-derived ectocervix organoids reveals distinct cellular reprogramming. *Nat Commun* (2022) 13:1030. doi: 10.1038/s41467-022-28569-1
- Chumduri C, Gurumurthy RK, Berger H, Dietrich O, Kumar N, Koster S, et al. Opposing Wnt signals regulate cervical squamocolumnar homeostasis and emergence of metaplasia. *Nat Cell Biol* (2021) 23:184–97. doi: 10.1038/s41556-020-00619-0
- Schönefeldt S, Wais T, Herling M, Mustjoki S, Bekiaris V, Moriggl R, et al. The diverse roles of $\gamma\delta$ T cells in cancer: from rapid immunity to aggressive lymphoma. *Cancers (Basel)* (2021) 13. doi: 10.3390/cancers13246212
- Mensurado S, Blanco-Domínguez R, Silva-Santos B. The emerging roles of $\gamma\delta$ T cells in cancer immunotherapy. *Nat Rev Clin Oncol* (2023) 20:178–91. doi: 10.1038/s41571-022-00722-1
- Kalyan S, Kabelitz D. Defining the nature of human $\gamma\delta$ T cells: a biographical sketch of the highly empathetic. *Cell Mol Immunol* (2013) 10:21–9. doi: 10.1038/cmi.2012.44
- Xu Y, Xiang Z, Alnaggar M, Kouakanou L, Li J, He J, et al. Allogeneic V γ 9V δ 2 T-cell immunotherapy exhibits promising clinical safety and prolongs the survival of patients with late-stage lung or liver cancer. *Cell Mol Immunol* (2021) 18:427–39. doi: 10.1038/s41423-020-0515-7
- Kabelitz D, Serrano R, Kouakanou L, Peters C, Kalyan S. Cancer immunotherapy with $\gamma\delta$ T cells: many paths ahead of us. *Cell Mol Immunol* (2020) 17:925–39. doi: 10.1038/s41423-020-0504-x
- Yazdanifar M, Barbarito G, Bertaina A, Airoidi I. $\gamma\delta$ T cells: the ideal tool for cancer immunotherapy. *Cells* (2020) 9. doi: 10.3390/cells9051305
- Harly C, Guillaume Y, Nedelec S, Peigné C-M, Mönkkönen H, Mönkkönen J, et al. Key implication of CD277/butyrophilin-3 (BTN3A) in cellular stress sensing by a major human $\gamma\delta$ T-cell subset. *Blood* (2012) 120:2269–79. doi: 10.1182/blood-2012-05-430470
- Karunakaran MM, Willcox CR, Salim M, Paletta D, Fichtner AS, Noll A, et al. Butyrophilin-2A1 directly binds germline-encoded regions of the V γ 9V δ 2 TCR and is essential for phosphoantigen sensing. *Immunity* (2020) 52:487–498.e486. doi: 10.1016/j.immuni.2020.02.014
- Rigau M, Ostrouska S, Fulford TS, Johnson DN, Woods K, Ruan Z, et al. Butyrophilin 2A1 is essential for phosphoantigen reactivity by $\gamma\delta$ T cells. *Science* (2020) 367:eaay5516. doi: 10.1126/science.aay5516
- Willcox CR, Salim M, Begley CR, Karunakaran MM, Easton EJ, Von Klotek C, et al. Phosphoantigen sensing combines TCR-dependent recognition of the BTN3A IgV domain and germline interaction with BTN2A1. *Cell Rep* (2023) 42:112321. doi: 10.1016/j.celrep.2023.112321
- Girardi M, Oppenheim DE, Steele CR, Lewis JM, Glusac E, Filler R, et al. Regulation of cutaneous malignancy by gammadelta T cells. *Science* (2001) 294:605–9. doi: 10.1126/science.1063916
- Silva-Santos B, Mensurado S, Coffelt SB. $\gamma\delta$ T cells: pleiotropic immune effectors with therapeutic potential in cancer. *Nat Rev Cancer* (2019) 19:392–404. doi: 10.1038/s41568-019-0153-5
- Itohara S, Mombaerts P, Lafaille J, Iacomini J, Nelson A, Clarke AR, et al. T cell receptor delta gene mutant mice: independent generation of alpha beta T cells and programmed rearrangements of gamma delta TCR genes. *Cell* (1993) 72:337–48. doi: 10.1016/0092-8674(93)90112-4
- Lertworapreecha M, Patumraj S, Niruthisard S, Hansasuta P, Bhattarakosol P. Cytotoxic function of gamma delta (gamma/delta) T cells against pamidronate-treated cervical cancer cells. *Indian J Exp Biol* (2013) 51:597–605.
- Giannattasio A, Weil S, Kloess S, Ansari N, Stelzer EHK, Cerwenka A, et al. Cytotoxicity and infiltration of human NK cells in *in vivo*-like tumor spheroids. *BMC Cancer* (2015) 15:351. doi: 10.1186/s12885-015-1321-y
- Gurumurthy RK, Koster S, Kumar N, Meyer TF, Chumduri C. Patient-derived and mouse endo-ectocervical organoid generation, genetic manipulation and applications to model infection. *Nat Protoc* (2022) 17:1658–90. doi: 10.1038/s41596-022-00695-6
- Schindelin J, Arganda-Carreras I, Frise E, Kaynig V, Longair M, Pietzsch T, et al. Fiji: an open-source platform for biological-image analysis. *Nat Methods* (2012) 9:676–82. doi: 10.1038/nmeth.2019
- Holthaus D, Delgado-Betancourt E, Aebischer T, Seeber F, Klotz C. Harmonization of protocols for multi-species organoid platforms to study the intestinal biology of toxoplasma gondii and other protozoan infections. *Front Cell Infect Microbiol* (2020) 10:610368. doi: 10.3389/fcimb.2020.610368
- Herfs M, Yamamoto Y, Laury A, Wang X, Nucci MR, McLaughlin-Drubin ME, et al. A discrete population of squamocolumnar junction cells implicated in the pathogenesis of cervical cancer. *Proc Natl Acad Sci USA* (2012) 109:10516–21. doi: 10.1073/pnas.1202684109
- Peters C, Kouakanou L, Oberg H-H, Wesch D, Kabelitz D. Chapter Eleven - *In vitro* expansion of V γ 9V δ 2 T cells for immunotherapy. In: Galluzzi L, Rudqvist N-P, editors. *Methods in Enzymology* (Cambridge, Massachusetts, United States: Academic Press) (2020). p. 223–37.
- Davodeau F, Peyrat MA, Hallet MM, Gaschet J, Houde I, Vivien R, et al. Close correlation between Daudi and mycobacterial antigen recognition by human gamma delta T cells and expression of V9JPC1 gamma/V2DJC delta-encoded T cell receptors. *J Immunol* (1993) 151:1214–23. doi: 10.4049/jimmunol.151.3.1214
- Sacchi A, Tumino N, Sabatini A, Cimini E, Casetti R, Bordoni V, et al. Myeloid-derived suppressor cells specifically suppress IFN-gamma production and antitumor cytotoxic activity of Vdelta2 T cells. *Front Immunol* (2018) 9:1271. doi: 10.3389/fimmu.2018.01271
- Kuroda Y, Wakao S, Kitada M, Murakami T, Nojima M, Dezawa M. Isolation, culture and evaluation of multilineage-differentiating stress-enduring (Muse) cells. *Nat Protoc* (2013) 8:1391–415. doi: 10.1038/nprot.2013.076
- Hedemann N, Herz A, Schiepanski JH, Dittich J, Sebens S, Dempfle A, et al. ADAM17 inhibition increases the impact of cisplatin treatment in ovarian cancer spheroids. *Cancers (Basel)* (2021) 13. doi: 10.3390/cancers13092039
- Dekkers JF, Alieva M, Cleven A, Keramati F, Wezenaar AKL, Van Vliet EJ, et al. Uncovering the mode of action of engineered T cells in patient cancer organoids. *Nat Biotechnol* (2022) 41(1):60–9. doi: 10.1038/s41587-022-01397-w
- Dobin A, Davis CA, Schlesinger F, Drenkow J, Zaleski C, Jha S, et al. STAR: ultrafast universal RNA-seq aligner. *Bioinformatics* (2013) 29:15–21. doi: 10.1093/bioinformatics/bts635
- Frankish A, Diekhans M, Ferreira AM, Johnson R, Jungreis I, Loveland J, et al. GENCODE reference annotation for the human and mouse genomes. *Nucleic Acids Res* (2019) 47:D766–d773. doi: 10.1093/nar/gky955
- Love MI, Huber W, Anders S. Moderated estimation of fold change and dispersion for RNA-seq data with DESeq2. *Genome Biol* (2014) 15:550. doi: 10.1186/s13059-014-0550-8
- R Core Team. *R: A language and environment for statistical computing*. Vienna, Austria: R Foundation for Statistical Computing (2021).
- Yu G, Wang LG, Han Y, He QY. clusterProfiler: an R package for comparing biological themes among gene clusters. *Omic* (2012) 16:284–7. doi: 10.1089/omi.2011.0118
- Liberzon A, Subramanian A, Pinchback R, Thorvaldsdóttir H, Tamayo P, Mesirov JP. Molecular signatures database (MSigDB) 3.0. *Bioinformatics* (2011) 27:1739–40. doi: 10.1093/bioinformatics/btr260
- Ahmed HG, Bensumaidea SH, Alshammari FD, Alenazi FSH, Ba AL, Alturkstani MZ, et al. Prevalence of Human Papillomavirus subtypes 16 and 18 among Yemeni Patients with Cervical Cancer. *Asian Pac J Cancer Prev* (2017) 18:1543–8. doi: 10.22034/apjcp.2017.18.6.1543
- Dai Y, Chen H, Mo C, Cui L, He W. Ectopically expressed human tumor biomarker MutS homologue 2 is a novel endogenous ligand that is recognized by human $\gamma\delta$ T cells to induce innate anti-tumor/virus immunity. *J Biol Chem* (2012) 287:16812–9. doi: 10.1074/jbc.M111.327650
- Xiang Z, Tu W. Dual face of Vgamma9Vdelta2-T cells in tumor immunology: anti-versus pro-tumoral activities. *Front Immunol* (2017) 8:1041. doi: 10.3389/fimmu.2017.01041
- Mo C, Dai Y, Kang N, Cui L, He W. Ectopic Expression of Human MutS Homologue 2 on Renal Carcinoma Cells Is Induced by Oxidative Stress with Interleukin-18 Promotion via p38 Mitogen-activated Protein Kinase (MAPK) and c-Jun N-terminal Kinase (JNK) Signaling Pathways. *J Biol Chem* (2012) 287:19242–54. doi: 10.1074/jbc.M112.349936
- Chen H, Ji X, Cui L, Zhang J, He W. Characterization of complementary determinant region 3 δ in human MutS homologue 2-specific $\gamma\delta$ T cells. *Scand J Immunol* (2015) 81:121–8. doi: 10.1111/sji.12256
- Ma W, Liang J, Mo J, Zhang S, Hu N, Tian D, et al. Butyrophilin-like 9 expression is associated with outcome in lung adenocarcinoma. *BMC Cancer* (2021) 21:1096. doi: 10.1186/s12885-021-08790-9
- Mo Q, Xu K, Luo C, Zhang Q, Wang L, Ren G. BTNL9 is frequently downregulated and inhibits proliferation and metastasis via the P53/CDC25C and P53/GADD45 pathways in breast cancer. *Biochem Biophys Res Commun* (2021) 553:17–24. doi: 10.1016/j.bbrc.2021.03.022
- Iwasaki M, Tanaka Y, Kobayashi H, Murata-Hirai K, Miyabe H, Sugie T, et al. Expression and function of PD-1 in human $\gamma\delta$ T cells that recognize phosphoantigens. *Eur J Immunol* (2011) 41:345–55. doi: 10.1002/eji.201040959
- Wang X, Zhao Y, Zou X, Wang L. Relationship of P16 and Ki67 in recurrence of HPV infection and cervical intraepithelial neoplasia. *Int J Clin Exp Pathol* (2020) 13:3174–80.

47. Herrmann T. Caveat: Monoclonal antibodies 20.1 and 103.2 bind all human BTN3A proteins and are not suited to study BTN3A1-specific features. *Proc Natl Acad Sci* (2023) 120:e2304065120. doi: 10.1073/pnas.2304065120
48. Yuan L, Ma X, Yang Y, Qu Y, Li X, Zhu X, et al. Phosphoantigens glue butyrophilin 3A1 and 2A1 to activate V γ 9V δ 2 T cells. *Nature* (2023) 621:840–8. doi: 10.1038/s41586-023-06525-3
49. Chen S, Li Z, Huang W, Wang Y, Fan S. Prognostic and therapeutic significance of BTN3A proteins in tumors. *J Cancer* (2021) 12:4505–12. doi: 10.7150/jca.57831
50. Zur Hausen H. Condylomata acuminata and human genital cancer. *Cancer Res* (1976) 36:794.
51. Shi Q, Xu L, Yang R, Meng Y, Qiu L. Ki-67 and P16 proteins in cervical cancer and precancerous lesions of young women and the diagnostic value for cervical cancer and precancerous lesions. *Oncol Lett* (2019) 18:1351–5. doi: 10.3892/ol.2019.10430
52. Caron J, Ridgley LA, Bodman-Smith M. How to train your dragon: harnessing gamma delta T cells antiviral functions and trained immunity in a pandemic era. *Front Immunol* (2021) 12. doi: 10.3389/fimmu.2021.666983
53. Raverdeau M, Cunningham SP, Harmon C, Lynch L. $\gamma\delta$ T cells in cancer: a small population of lymphocytes with big implications. *Clin Trans Immunol* (2019) 8:e01080. doi: 10.1002/cti2.1080
54. Dieli F, Vermijlen D, Fulfaro F, Caccamo N, Meraviglia S, Cicero G, et al. Targeting human gammadelta T cells with zoledronate and interleukin-2 for immunotherapy of hormone-refractory prostate cancer. *Cancer Res* (2007) 67:7450–7. doi: 10.1158/0008-5472.CAN-07-0199
55. Oberg HH, Kellner C, Gonnermann D, Sebens S, Bauerschlag D, Gramatzki M, et al. Tribody [(HER2)(2)xCD16] is more effective than trastuzumab in enhancing $\gamma\delta$ T cell and natural killer cell cytotoxicity against HER2-expressing cancer cells. *Front Immunol* (2018) 9:814. doi: 10.3389/fimmu.2018.00814
56. Duensing S, Lee LY, Duensing A, Basile J, Piboonnuyom S, Gonzalez S, et al. The human papillomavirus type 16 E6 and E7 oncoproteins cooperate to induce mitotic defects and genomic instability by uncoupling centrosome duplication from the cell division cycle. *Proc Natl Acad Sci USA* (2000) 97:10002–7. doi: 10.1073/pnas.170093297
57. Basukala O, Mittal S, Massimi P, Bestagno M, Banks L. The HPV-18 E7 CKII phospho acceptor site is required for maintaining the transformed phenotype of cervical tumour-derived cells. *PLoS Pathog* (2019) 15:e1007769. doi: 10.1371/journal.ppat.1007769
58. Amin FAS, Un Naher Z, Ali PSS. Molecular markers predicting the progression and prognosis of human papillomavirus-induced cervical lesions to cervical cancer. *J Cancer Res Clin Oncol* (2023) 149(10):8077–86. doi: 10.1007/s00432-023-04710-5
59. Chen D, Guo Y, Jiang J, Wu P, Zhang T, Wei Q, et al. $\gamma\delta$ T cell exhaustion: Opportunities for intervention. *J Leukocyte Biol* (2022) 112:1669–76. doi: 10.1002/JLB.5MR0722-777R
60. Gober H-JR, Kistowska M, Angman L, Jenö P, Mori L, De Libero G. Human T cell receptor $\gamma\delta$ Cells recognize endogenous mevalonate metabolites in tumor cells. *J Exp Med* (2003) 197:163–8. doi: 10.1084/jem.20021500
61. Hirsh MI, Junger WG. Roles of heat shock proteins and gamma delta T cells in inflammation. *Am J Respir Cell Mol Biol* (2008) 39:509–13. doi: 10.1165/rcmb.2008-0090TR
62. Li R, Qian J, Zhang W, Fu W, Du J, Jiang H, et al. Human heat shock protein-specific cytotoxic T lymphocytes display potent antitumor immunity in multiple myeloma. *Br J Haematol* (2014) 166:690–701. doi: 10.1111/bjh.12943
63. Zumwalde NA, Haag JD, Sharma D, Mirrieles JA, Wilke LG, Gould MN, et al. Analysis of immune cells from human mammary ductal epithelial organoids reveals V δ 2+ T cells that efficiently target breast carcinoma cells in the presence of bisphosphonate. *Cancer Prev Res (Phila)* (2016) 9:305–16. doi: 10.1158/1940-6207.CAPR-15-0370-T
64. King LA, Toffoli EC, Veth M, Iglesias-Guimaras V, Slot MC, Amsen D, et al. A Bispecific $\gamma\delta$ T-cell Engager Targeting EGFR Activates a Potent V γ 9V δ 2 T cell-Mediated Immune Response against EGFR-Expressing Tumors. *Cancer Immunol Res* (2023) 11:1237–52. doi: 10.1158/2326-6066.CIR-23-0189
65. De Gassart A, Le KS, Brune P, Agaugué S, Sims J, Goubard A, et al. Development of ICT01, a first-in-class, anti-BTN3A antibody for activating V γ 9V δ 2 T cell-mediated antitumor immune response. *Sci Transl Med* (2021) 13:eabj0835. doi: 10.1126/scitranslmed.abj0835